GEOPHYSICAL RESEARCH LETTERS, VOL. 34, L04810, doi:10.1029/2006GL028284, 2007

Tropospheric vertical distribution of tropical Atlantic ozone observed by TES during the northern African biomass burning season

L. Jourdain,[1] H. M. Worden,[1] J. R. Worden,[1] K. Bowman,[1] Q. Li,[1] A. Eldering,[1] S. S. Kulawik,[1] G. Osterman,[1] K. F. Boersma,[2] B. Fisher,[1] C. P. Rinsland,[3] R. Beer,[1] and M. Gunson[1]

Received 25 September 2006; revised 15 November 2006; accepted 1 December 2006; published 23 February 2007.

[1] We present vertical distributions of ozone from the Tropospheric Emission Spectrometer (TES) over the tropical Atlantic Ocean during January 2005. Between 10N and 20S, TES ozone retrievals have Degrees of Freedom for signal (DOF) around 0.7–0.8 each for tropospheric altitudes above and below 500 hPa. As a result, TES is able to capture for the first time from space a distribution characterized by two maxima: one in the lower troposphere north of the ITCZ and one in the middle and upper troposphere south of the ITCZ. We focus our analysis on the north tropical Atlantic Ocean, where most of previous satellite observations showed discrepancies with in-situ ozone observations and models. Trajectory analyses and a sensitivity study using the GEOS-Chem model confirm the influence of northern Africa biomass burning on the elevated ozone mixing ratios observed by TES over this region. **Citation:** Jourdain, L., et al. (2007), Tropospheric vertical distribution of tropical Atlantic ozone observed by TES during the northern African biomass burning season, *Geophys. Res. Lett.*, *34*, L04810, doi:10.1029/2006GL028284.

1. Introduction

[2] In situ observations from ship cruise campaigns [*Weller et al.*, 1996; *Thompson et al.*, 2000] and model studies [*Edwards et al.*, 2003; *Martin et al.*, 2002] show that the early year tropospheric ozone distribution over the tropical Atlantic Ocean is characterized by two maxima: one in the lower troposphere north of the Intertropical Convergence Zone (ITCZ) and one in the middle and upper troposphere south of the ITCZ. The first one is attributed to the biomass burning occurring at this time of the year over Africa north of the Equator [*Thompson et al.*, 2000]. The latter one is attributed to a combination of lightning NO_x emissions, various transport processes (including subsidence, convection, cross-equatorial transport and stratospheric intrusions) and photochemistry [e.g., *Thompson et al.*, 2000; *Moxim and Levy*, 2000; *Edwards et al.*, 2003; *Martin et al.*, 2002; *Chatfield et al.*, 2004]. The previous satellite view of the tropospheric ozone over the tropical Atlantic is based on the distribution of the tropical tropospheric ozone columns (TTOCs) derived by different methods from the Total Ozone Mapping Spectrometer (TOMS) observations [e.g., *Fishman and Larsen*, 1987; *Fishman et al.*, 1991; *Ziemke et al.*, 1998; *Thompson and Hudson*, 1999; *Kim et al.*, 2001]. This vertically integrated view exhibits several features in agreement with in-situ observations over the tropical Atlantic Ocean. In particular, these products present a persistent zonal wave-one pattern over the Southern Hemisphere with a maximum over the Atlantic, a minimum over the western Pacific, and a maximum amplitude during the austral dry season in agreement with in situ observations [*Thompson and Hudson*, 1999; *Thompson et al.*, 2003]. In addition, most of these products show higher TTOCs over the south tropical Atlantic than over the north Atlantic during the northern Africa biomass burning season. This is called the ''Tropical Atlantic Ozone Paradox'' and was first revealed by in situ measurements from ship cruise campaigns [*Thompson et al.*, 2000]. However, most of the TOMS TTOCs products over northern Africa during the biomass burning season, except for those of *Kim et al.* [2001, 2005], do not capture the seasonal ozone enhancement of the TTOCs as found in the in-situ observations and model simulations and show a minimum in DJF and a maximum in SON. This discrepancy is due to the low sensitivity of TOMS to the lower troposphere and would lead to increase the magnitude of the ''Tropical Atlantic Ozone Paradox'' [*Martin et al.*, 2002]. The more recent TTOCs products from the Global Ozone Monitoring Experiment (GOME) also show some discrepancies with models and measurements over northern Africa, presenting no clear seasonal cycle [*Valks et al.*, 2003; *Liu et al.*, 2006].

[3] In this paper, we present the first satellite observations of the vertical variation of tropospheric ozone over the tropical Atlantic Ocean. We focus our analysis on the TES retrievals over the northern part of the tropical Atlantic Ocean, where the previous satellite observations derived from TOMS (except those of *Kim et al.* [2001, 2005]) show some discrepancies with the in-situ ozone observations and models.

2. TES Data

[4] The TES instrument is an infrared Fourier transform spectrometer with a spectral resolution of 0.1 cm^{-1} and a spectral range from 650–2250 cm^{-1} [*Beer et al.*, 2001] launched aboard the NASA's Aura satellite in July 2004. Standard products are vertical profiles of ozone, CO and water vapor obtained from nadir observations during the Global Survey and Step and Stare runs. A Global Survey

[1]Jet Propulsion Laboratory, California Institute of Technology, Pasadena, California, USA.
[2]Department of Earth and Planetary Science and Division of Engineering and Applied Sciences, Harvard University, Cambridge, Massachusetts, USA.
[3]NASA Langley Research Center, Hampton, Virginia, USA.

0094-8276/07/2006GL028284$05.00

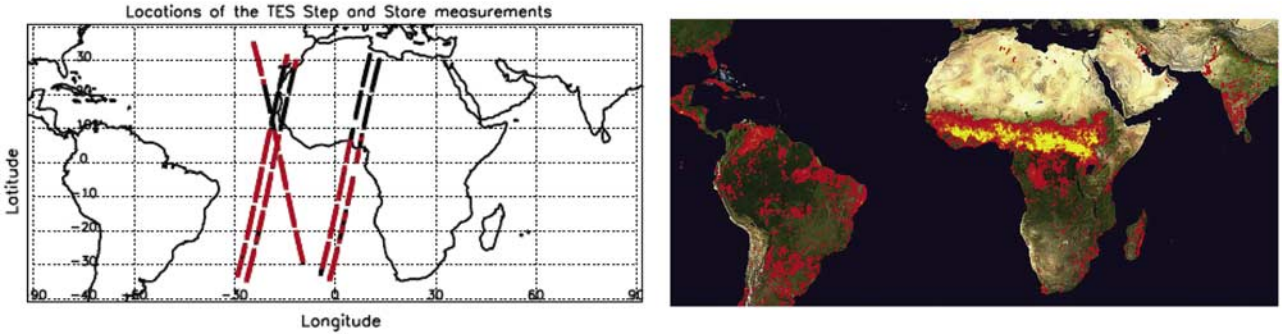

Figure 1. (left) Measurement locations of the 5 TES Special Observations considered in this study. Locations shown in red indicate retrievals used in the analysis. (right) Spatial distribution of the fires detected by MODIS during the period 11–21 January 2005 [*Giglio et al.*, 2003]. Colors range from red where the fire count is low to yellow where number of fires is large.

run consists of nadir measurements about 5° apart along the orbit track, with successive orbits 22° apart in longitude. Step/Stare runs have denser nadir coverage, about 0.4° apart, and typically covers a 60° latitude range. The vertical resolution of TES nadir ozone retrievals is about 6 km for cloud-free scenes, with sensitivity to both the lower and upper troposphere [*Worden et al.*, 2004; *Bowman et al.*, 2006]. The TES ozone retrievals have been evaluated using ozonesonde measurements by *Worden et al.* [2007]. The algorithm used for retrieving the vertical trace gas profiles from TES radiances is based on an optimal estimation method [*Rodgers*, 2000] and is described by *Worden et al.* [2004] and *Bowman et al.* [2006]. The relationship between elements of the true trace gas profile and of the retrieved profile can be expressed as:

$$\hat{\mathrm{x}} = \mathbf{x_a} + \mathbf{A}(\mathbf{x} - \mathbf{x_a}) + \mathbf{G}\boldsymbol{\varepsilon} \quad (1)$$

where $\hat{\mathrm{x}}$ is the logarithm of the retrieved profile, $\mathbf{x_a}$ is the logarithm of the a priori constraint obtained from monthly mean profiles simulated with the MOZART-3 model and binned in 10° latitude × 60° longitude grids, $\mathbf{x}$ is the logarithm of the true profile, ε is the radiance measurement noise, and $\mathbf{G}$ is the gain matrix converting the noise to spectral measurement error. The averaging kernel ($\mathbf{A}$) describes the sensitivity of the retrieved profile to the perturbations of the true state.

[5] In this study, we use TES ozone profiles (version V002, F03_2) from 5 Step and Stare runs covering the period 22–25 January 2005. These data are selected based on a set of quality flags described in detail by *Osterman* [2006]. It is important to note that we also exclude observations over the Sahara desert, where the surface emissivity has strong silicate features, as well as profiles that exhibit a persistent emission layer near the surface with atmospheric temperatures higher than the surface temperature. Both of these conditions can cause extreme non-linearity in the retrieval algorithm, and can produce erroneous ozone estimates. Variable cloud and aerosol conditions are also present for these observations. The scheme used in the retrieval algorithm to account for clouds relies on spectrally dependent effective optical depths as well as cloud top pressure that are retrieved in concert with the gases. The scheme is generalized, so a single layer cloud or aerosol with spectral features that are at least 25 cm^{-1} wide will be properly accommodated in the TES retrieval scheme. The cases that cannot be accommodated by the cloud retrieval scheme generally result in very high radiance residual RMS values that are screened out in the quality control step. Although clouds and aerosols affect the vertical sensitivity of TES, as captured by the averaging kernel provided with each retrieval, it has been shown that they do not bias TES ozone estimates [*Kulawik et al.*, 2006]. The locations of the TES retrievals used for this study are shown in red in Figure 1. Total errors estimates, including smoothing, systematic, cross-state, and measurements errors, are given for each profile and range from 15 to 35%.

3. GEOS-Chem Model

[6] We use the GEOS-Chem v7.02.04 global 3-D tropospheric chemistry and transport model with a horizontal resolution of 2° × 2.5° and 55 layers in the vertical (available at http://www-as.harvard.edu/chemistry/trop/geos/). This model has been described by *Park et al.* [2004] and a simulation driven by the assimilated meteorological GEOS-4 data from the NASA Global Modeling and Assimilation Office (GMAO) has been recently globally evaluated by *Wu et al.* [2007]. For this study, we have performed a simulation for the period September 2004–January 2005 driven by the GEOS-4 data updated every 3–6 hours. Biomass burning emissions are from a monthly climatology [*Lobert et al.*, 1999; *Duncan et al.*, 2003] and are redistributed for each day of the simulation according to the daily fires detected by the MOderate Resolution Imaging Spectroradiometer (MODIS). To study the influence of the biomass burning emissions from northern Africa on the ozone concentrations observed by TES, we have also performed an additional simulation with the GEOS-Chem model, in which the biomass burning emissions over this region have been turned off.

4. TES Ozone Latitudinal Cross Section, Comparison With the GEOS-Chem Model, and Previous In Situ Measurements

[7] For comparisons with TES, the model profiles are sampled along the Aura orbit track at the observation times,

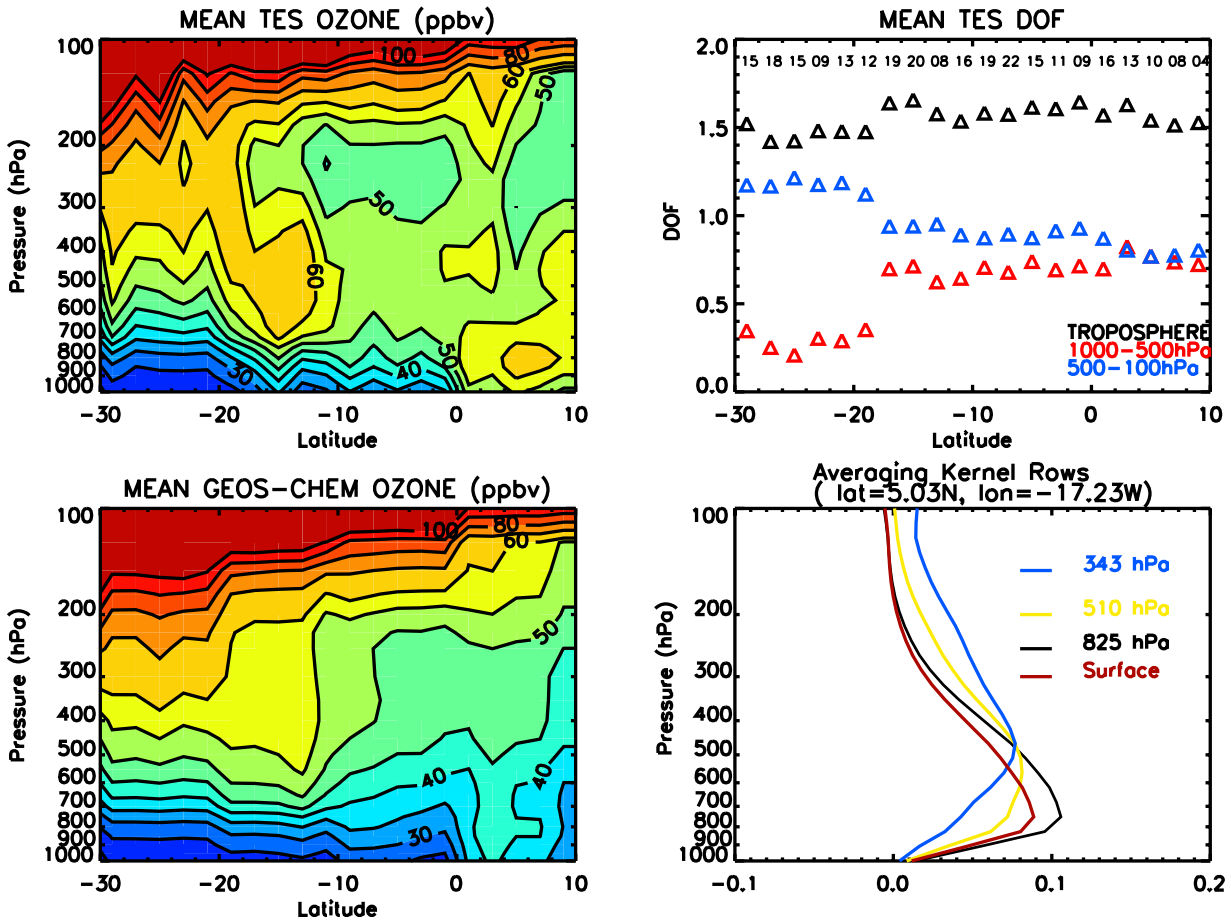

Figure 2. (left) Cross section pressure-latitude of mean ozone volume mixing ratio retrieved by (top) TES and (bottom) simulated by GEOS-Chem for the period 22–25 January 2005 over the tropical Atlantic Ocean. Note that we show the TES retrievals on the radiative transfer model levels, which should not be construed as independent. (right top) Latitudinal variation of the DOF for TES ozone retrievals for the whole troposphere (black triangles), the surface-500 hPa region (red triangles), the 500 hPa–100 hPa region (blue triangles). The number of TES vertical profiles averaged in each latitude band of 2 degrees is also indicated in this plot. (right bottom) Rows of the averaging kernel for different levels for a particular retrieval of the region I (latitude, 5.03; longitude, −17.23).

and interpolated onto the TES pressure grid. In order to take into account the vertical sensitivity of each TES retrieval, the model profiles are transformed using the TES observation operator, which is composed of the averaging kernel and the a priori profile and is equivalent to equation (1) without the gain matrix [*Worden et al.*, 2007]. As described by *Bowman et al.* [2006], differences between TES and GEOS-Chem are compared to TES reported observational errors (sum of the measurement and cross-state errors estimates). Figure 2 shows the latitudinal cross sections of the mean tropospheric ozone mixing ratios over the tropical Atlantic Ocean derived from the TES retrievals and the corresponding GEOS-Chem profiles. To account for the model resolution, the profiles have been averaged over bands of 2 degrees in latitude for this comparison (the number of profiles used for the average are indicated in Figure 2). The ozone distribution observed by TES can be separated into three regions. Between 0 and 10 N (region I), the TES ozone vertical distribution exhibits a maximum of 60–70 ppbv in the lower troposphere below 600 hPa. South of this region down to 20 S (region II), TES observes lower ozone mixing ratios (40 ppbv) in the lower troposphere and higher ozone mixing ratios (70 ppbv) in the middle troposphere compared to the region I especially between 10S and 20 S. Between 20S and 30S (region III), a maximum of 70–80 ppbv appears in the upper troposphere above 400 hPa. The separation in 3 distinct regions is in agreement with the analysis of the ozonesonde measurements during the Aerosols 99 experiment between 14 N and 30 S [*Thompson et al.*, 2000, Figure 1]. In particular, the TES ozone profiles exhibit a maximum in the middle troposphere south of the equator as well as a maximum in the lower troposphere north of the equator. As a result, the latitudinal ozone gradients observed by TES in the lower and middle/upper troposphere are reversed, as they are in the in-situ observations. We have calculated the degrees of freedom for signal (DOF), as defined by *Rodgers* [2000], to quantify TES vertical sensitivity to real atmospheric variability. The DOF for the whole tropospheric profile varies between 1.5 and 1.7 over a latitude range of 30S to 10N as shown in Figure 2. Between 10N–18S, the middle/upper tropospheric (500 hPa to tropopause) as well as the lower tropospheric (surface to

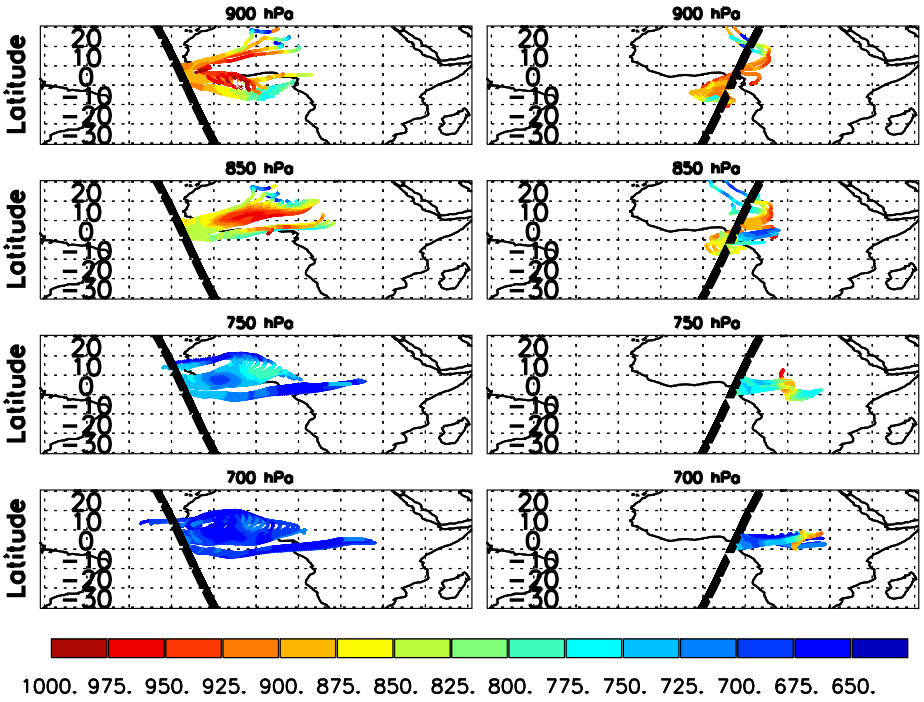

Figure 3. Seven-day backward trajectories initialized from the location and time of two TES Step and Stare between 0–10 N and at 900, 850, 750 and 700 hPa. The color scale represents the pressure of the air masses along the trajectories.

500h Pa) part of the retrievals have a DOF of about 0.7–0.8 each. This suggests that TES can distinguish between lower and upper tropospheric ozone as well as provide a reasonable estimate of the ozone abundance in the lower troposphere between 10N–18S. Figure 2 also shows the rows from typical averaging kernel for one of the retrievals that contribute to the enhanced ozone below 600 hPa north of the equator. The structure of the averaging kernel reveals that most of the information in the retrieval below 500 hPa comes from around 700 hPa altitude, where TES sensitivity for tropospheric ozone is at a maximum. We also note that these TES retrievals show significant differences from the TES a priori profiles (not shown, discussed in the auxiliary material).[1] This is further confirmation that TES observations add new information to the a priori knowledge in the troposphere, as expected based on the vertical sensitivity characterized in each retrieval. The latitudinal and vertical ozone variation over the tropical Atlantic Ocean simulated by the GEOS-Chem model is in qualitative agreement with the TES observations. However, the maxima of the simulated distribution are generally weaker. In particular, GEOS-Chem is lower than TES on average by 20–25 ppbv between 0–10N (region I). This difference is larger than the TES observational errors (less than 15 ppbv for an individual profile) as well as the variability of TES and GEOS-Chem in this region, 15 and 8 ppbv respectively (not shown), indicating that the difference is statistically significant. This result is consistent with the underestimation by 30% of the ozone mixing ratios over northern Africa (Abidjan and Lagos) in our simulation compared to a climatology derived from the MOZAIC measurements by *Sauvage et al.* [2005] (not shown). It is important to note that similar discrepancies between the ozone mixing ratios simulated by the GEOS-Chem model and in situ measurements in the regions influenced by biomass burning activity have been found by *Martin et al.* [2002] for the northern Africa and by *Sinha et al.* [2004] for the southern Africa. These discrepancies in close vicinity of fires could be explained by the coarse resolution of the model as suggested by *Sinha et al.* [2004] or, more likely, by an underestimation of the NO_x emissions from biomass burning in the GEOS-Chem model. Inverse modeling studies using the NO_2 columns from GOME observations and the GEOS-Chem model [*Martin et al.*, 2003; *Jaeglé et al.*, 2005] suggest that the biomass burning NO_x emissions in northern equatorial Africa in the GEOS-Chem model are underestimated, by as much as 50% [*Jaeglé et al.*, 2005].

5. Factors Influencing the TES Ozone Distribution in Region I (0 to10 N)

[8] We now focus on the measurements in region I where previous satellite measurements of tropospheric ozone have been problematic due to less sensitivity to ozone variations in the lower troposphere [*Kim et al.*, 2005].

5.1. Trajectory Analysis

[9] We have calculated 7-day backward trajectories initialized from the location and time of the TES Step and Stare measurements over region I (0 to10 N) using the HYSPLIT transport and dispersion model (R. R. Draxler and G. D. Rolph, HYSPLIT (Hybrid Single-Particle Lagrangian Integrated Trajectory) model, 2003, available at http://www.arl.noaa.gov/ready/open/hysplit4.html) driven

[1] Auxiliary materials are available in the HTML. doi:10.1029/2006GL028284.

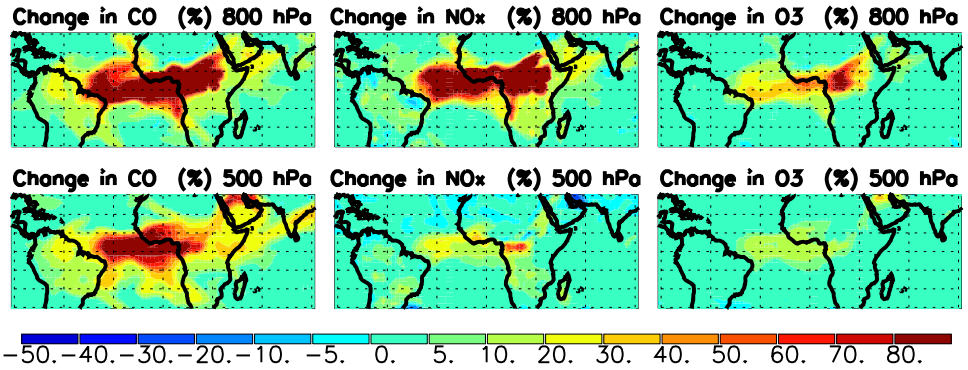

Figure 4. Changes in the simulated CO, NO_x, ozone mixing ratios fields (in percent) at 800 hPa (top) and 500 hPa (bottom) when the biomass burning emissions from northern Africa are considered in the GEOS-Chem model. These changes are relative to the simulation which does not include the biomass burning source.

by the NCEP/NCAR reanalysis. Figure 3 shows the results for 2 Step and Stare at 4 levels in the lower troposphere. At 900 hPa, the origin of the air is either oceanic and southerly or continental and northerly depending on the location of the measurements with respect to the ITCZ. At 850 hPa, off the West Africa Coast northeasterly winds (i.e.: Harmattan winds) prevail and transport air masses from West Africa. During their travel westward and equatorward, these parcels rise from lower levels near the surface. This ascent is usually explained by the adiabatic lifting taking place when the parcels meet the cool monsoon layer [*Jonquières et al.*, 1998]. We have calculated that 98% of the parcels arriving at the location of the 3 Step and Stare measurements off the West Africa Coast at 850 hPa passed less than 7 days before over northern Africa below 900 hPa and south of 15 N (which is here considered as the northern limit of the fires region). Over the Gulf of Guinea, the trajectories initialized at the level 850 hPa present the same pattern than those initialized at 900 hPa, most of the parcels having an oceanic and southerly origin. At 750 hPa, over the Gulf of Guinea, easterly winds (i.e.: African Easterly Jet) bring air parcel of continental origin at the TES locations between 0–10N. These parcels rose from lower levels over Central Africa. In this case, the convective transport could be responsible for this initial lifting as suggested by the analysis of the outgoing longwave radiation (not shown). At 700 hPa, the circulation is dominated by the presence of an anticyclone centered at around 10 N, 15 W and the African Easterly Jet. As a result, the flow is principally horizontal and easterly. Overall, this analysis confirms that the air parcels in the ozone enhanced layer detected by TES around 800 hPa over the north tropical Atlantic Ocean have their origin several days before over west Africa and central Africa at lower altitudes where intensive biomass burning occurs at this period of the year (see Figure 1).

5.2. Interpretation With the GEOS-Chem Model

[10] The CO, NO_x and O_3 concentration changes calculated by the model when biomass burning emissions are included in the simulation are shown in Figure 4 for the 800 hPa and 500 hPa levels. CO mixing ratios increase by 90% over the source region as well as over north tropical Atlantic between 0–10 N at 800 hPa. The influence of the biomass burning activity decreases with altitude, but it still contributes around 50% at 300 hPa. The impact of this source on NO_x concentrations in the free troposphere remains limited because the NO_x has a short lifetime in the lower troposphere (~1 day). Ozone also has a relatively short lifetime in the boundary layer (less than a week). The ozone mixing ratios increase up to 80% over the source region. However, the changes in ozone concentrations decrease rapidly with decreasing longitude: 50% to 30% from the Gulf of Guinea to west of the north Atlantic basin for 0 to 10 N. Ozone from this source also decreases very rapidly with the altitude, the impact is about 10–20% at 500 hPa and less than 10% at 300 hPa. For the regions where TES observes enhanced ozone, the Gulf of Guinea and off the coast of west Africa, the GEOS-Chem model predicts that biomass burning emissions contribute to increase the lower tropospheric ozone background by 40–50% and by 20–30% respectively.

6. Conclusions

[11] The TES measurements presented in this paper constitute the first observation from space of a vertical distribution resolving lower and upper tropospheric ozone over the tropical Atlantic Ocean during the northern Africa biomass burning season. The TES distribution is in qualitative agreement with previous in situ measurements and models showing two maxima: one in the lower troposphere north of the ITCZ and one in the middle and upper troposphere south of the ITCZ. In this paper, we have focused on the TES measurements over the northern tropical Atlantic where enhanced ozone in the lower troposphere has been difficult to retrieve from previous space measurements. For this region, TES ozone retrievals exhibit an ozone enriched layer below 600 hPa, corresponding to the Harmattan layer, also observed by in situ observations over the tropical Atlantic [*Thompson et al.*, 2000], the Ivory Coast [*Jonquières et al.*, 1998], and from regular measurements over west Africa [*Sauvage et al.*, 2005]. A sensitivity study conducted with the GEOS-Chem model confirmed the influence of the biomass burning over western and central Africa on the ozone enriched layer observed by TES.

[12] **Acknowledgments.** This work was performed at the Jet Propulsion Laboratory, California Institute of Technology, under a contract with the National Aeronautics and Space Administration. We are grateful to

the NOAA Air Resources Laboratory (ARL) for the provision of the HYSPLIT transport and dispersion model (http://www.arl.noaa.gov/ready/hysplit4.html) and to the NASA/GSFC MODIS Rapid Response Project (http://rapidfire.sci.gsfc.nasa.gov/) for the provision of fire maps.

References

Beer, R., et al. (2001), Tropospheric Emission Spectrometer for the Earth Observing System's Aura satellite, *Appl. Opt.*, *40*, 2356–2367.

Bowman, K. W., et al. (2006), Tropospheric Emission Spectrometer: Retrieval method and error analysis, *IEEE Trans. Geosci. Remote Sens.*, *44, 1297–1307.*

Chatfield, R. B., H. Guan, A. M. Thompson, and J. C. Witte (2004), Convective lofting links Indian Ocean air pollution to paradoxical South Atlantic ozone maxima, *Geophys. Res. Lett.*, *31*, L06103, doi:10.1029/2003GL018866.

Duncan, B. N., R. V. Martin, A. C. Staudt, R. Yevich, and J. A. Logan (2003), Interannual and seasonal variability of biomass burning emissions constrained by satellite observations, *J. Geophys. Res.*, *108*(D2), 4100, doi:10.1029/2002JD002378.

Edwards, D. P., et al. (2003), Tropospheric ozone over the tropical Atlantic: A satellite perspective, *J. Geophys. Res.*, *108*(D8), 4237, doi:10.1029/2002JD002927.

Fishman, J., and J. C. Larsen (1987), Distribution of total ozone and stratospheric ozone in the tropics: Implications for the distribution of tropospheric ozone, *J. Geophys. Res.*, *92*, 6627–6634.

Fishman, J., et al. (1991), Identification of widespread pollution in the Southern Hemisphere deduced from satellite analysis, *Science*, *252*, 1693–1696.

Giglio, L., J. Descloitres, C. O. Justice, and Y. J. Kaufman (2003), An enhanced contextual fire detection algorithm for MODIS, *Remote Sens. Environ.*, *87*, 273–282.

Jaeglé, L., L. Steinberger, R. V. Martin, and K. Chance (2005), Global partitioning of NO_x sources using satellite observations: Relative roles of fossil fuel combustion, biomass burning and soil emissions, *Faraday Discuss.*, *130*, 407–423, doi:10.1039/b502128f.

Jonquières, I., A. Marenco, A. Maalej, and F. Rohrer (1998), Study of ozone formation and transatlantic transport from biomass burning emissions over West Africa during the airborne tropospheric ozone campaigns TROPOZ I and TROPOZ II, *J. Geophys. Res.*, *103*, 19,059–19,073.

Kim, J. H., et al. (2001), Distribution of tropical tropospheric ozone determined by the scan-angle method applied to TOMS measurement, *J. Atmos. Sci.*, *58*, 2699–2708.

Kim, J. H., S. Na, M. J. Newchurch, and R. V. Martin (2005), Tropical tropospheric ozone morphology and seasonality seen in satellite and in situ measurements and model calculations, *J. Geophys. Res.*, *110*, D02303, doi:10.1029/2003JD004332.

Kulawik, S. S., J. Worden, A. Eldering, K. Bowman, M. Gunson, G. B. Osterman, L. Zhang, S. A. Clough, M. W. Shephard, and R. Beer (2006), Implementation of cloud retrievals for Tropospheric Emission Spectrometer (TES) atmospheric retrievals: part I. Description and characterization of errors on trace gas retrievals, *J. Geophys. Res.*, *111*, D24204, doi:10.1029/2005JD006733.

Liu, X., et al. (2006), First directly retrieved global distribution of tropospheric column ozone from GOME: Comparison with the GEOS-CHEM model, *J. Geophys. Res.*, *111*, D02308, doi:10.1029/2005JD006564.

Lobert, J., W. C. Keene, J. A. Logan, and R. Yevich (1999), Global chlorine emissions from biomass burning: Reactive Chlorine Emission Inventory, *J. Geophys. Res.*, *104*(D7), 8373–8390.

Martin, R. V., et al. (2002), Interpretation of TOMS observations of tropical tropospheric ozone with a global model and in situ observations, *J. Geophys. Res.*, *107*(D18), 4351, doi:10.1029/2001JD001480.

Martin, R. V., D. J. Jacob, K. Chance, T. P. Kurosu, P. I. Palmer, and M. J. Evans (2003), Global inventory of nitrogen oxide emissions constrained by space-based observations of NO_2 columns, *J. Geophys. Res.*, *108*(D17), 4537, doi:10.1029/2003JD003453.

Moxim, W. J., and H. Levy II (2000), A model analysis of the tropical South Atlantic Ocean tropospheric ozone maximum: The interaction of transport and chemistry, *J. Geophys. Res.*, *105*, 17,393–17,416.

Osterman, G. (Ed.) (2006), TES L2 data user's guide, version 1.00, Jet Propul. Lab., Pasadena, Calif., 11 Apr. (Available at http://tes.jpl.nasa.gov/docsLinks/documents.cfm)

Park, R. J., D. J. Jacob, B. D. Field, R. M. Yantosca, and M. Chin (2004), Natural and transboundary pollution influences on sulfate-nitrate-ammonium aerosols in the United States: Implications for policy, *J. Geophys. Res.*, *109*, D15204, doi:10.1029/2003JD004473.

Rodgers, C. D. (2000), *Inverse Methods for Atmospheric Sounding: Theory and Practice*, World Sci., Hackensack, N. J.

Sauvage, B., et al. (2005), Tropospheric ozone over equatorial Africa: Regional aspects from the MOZAIC data, *Atmos. Chem. Phys.*, *5*, 311–335.

Sinha, P., L. Jaeglé, P. V. Hobbs, and Q. Liang (2004), Transport of biomass burning emissions from southern Africa, *J. Geophys. Res.*, *109*, D20204, doi:10.1029/2004JD005044.

Thompson, A. M., and R. D. Hudson (1999), Tropical tropospheric ozone (TTO) maps from Nimbus 7 and Earth Probe TOMS by the modified-residual method: Evaluation with sondes, ENSO signals, and trends from Atlantic regional time series, *J. Geophys. Res.*, *104*, 26,961–26,975.

Thompson, A. M., B. G. Doddridge, J. C. Witte, R. D. Hudson, W. T. Luke, J. E. Johnson, B. J. Johnson, S. J. Oltmans, and R. Weller (2000), A tropical Atlantic paradox: Shipborad and satellite views of a tropospheric ozone maximum and wave-one pattern in January–February 1999, *Geophys. Res. Lett.*, *27*, 3317–3320.

Thompson, A. M., et al. (2003), Southern Hemisphere Additional Ozonesondes (SHADOZ) 1998–2000 tropical ozone climatology: 2. Tropospheric variability and the zonal wave-one, *J. Geophys. Res.*, *108*(D2), 8241, doi:10.1029/2002JD002241.

Valks, P. J. M., R. B. A. Koelemeijer, M. van Weele, P. van Velthoven, J. P. F. Fortuin, and H. Kelder (2003), Variability in tropical tropospheric ozone: Analysis with Global Ozone Monitoring Experiment observations and a global model, *J. Geophys. Res.*, *108*(D11), 4328, doi:10.1029/2002JD002894.

Weller, R., R. Lilischkis, O. Schrems, R. Neuber, and S. Wessel (1996), Vertical ozone distribution in the marine atmosphere over the central Atlantic Ocean (56°S–50°N), *J. Geophys. Res.*, *101*, 1387–1399.

Worden, H. M., et al. (2007), Comparisons of Tropospheric Emission Spectrometer (TES) ozone profiles to ozonesondes: Methods and initial results, *J. Geophys. Res.*, doi:10.1029/2006JD007258, in press.

Worden, J., S. S. Kulawik, M. W. Shephard, S. A. Clough, H. Worden, K. Bowman, and A. Goldman (2004), Predicted errors of tropospheric emission spectrometer nadir retrievals from spectral window selection, *J. Geophys. Res.*, *109*, D09308, doi:10.1029/2004JD004522.

Wu, S., L. J. Mickley, D. J. Jacob, J. A. Logan, R. M. Yantosca, and D. Rind (2007), Why are there large differences between models in global budgets of tropospheric ozone?, *J. Geophys. Res.*, doi:10.1029/2006JD007801, in press.

Ziemke, J. R., S. Chandra, and P. K. Bhartia (1998), Two new methods for deriving tropospheric column ozone from TOMS measurements: Assimilated UARS MLS/HALOE and convective-cloud differential techniques, *J. Geophys. Res.*, *103*, 22,115–22,127.

R. Beer, K. Bowman, A. Eldering, B. Fisher, M. Gunson, L. Jourdain, S. S. Kulawik, Q. Li, G. Osterman, H. M. Worden, and J. R. Worden, Jet Propulsion Laboratory, California Institute of Technology, 4800 Oak Grove Drive, Pasadena, CA 91109, USA. (line.jourdain@jpl.nasa.gov)

K. F. Boersma, Department of Earth and Planetary Science and Division of Engineering and Applied Sciences, Harvard University, Pierce Hall, 29 Oxford Street, Cambridge, MA 02138, USA.

C. P. Rinsland, NASA Langley Research Center, Mail Stop 401A, 21 Langley Boulevard, Hampton, VA 23681-2199, USA.